Optics Letters

Slow light Mach–Zehnder interferometer as label-free biosensor with scalable sensitivity

Kun Qin,[1] Shuren Hu,[2] Scott T. Retterer,[3] Ivan I. Kravchenko,[3] and Sharon M. Weiss[1,2,*]

[1]Department of Electrical Engineering and Computer Science, Vanderbilt University, Nashville, Tennessee 37235, USA
[2]Department of Physics and Astronomy, Vanderbilt University, Nashville, Tennessee 37235, USA
[3]Center for Nanophase Materials Sciences, Oak Ridge National Laboratory, Oak Ridge, Tennessee 37831, USA
*Corresponding author: sharon.weiss@vanderbilt.edu

Received 26 November 2015; revised 30 December 2015; accepted 1 January 2016; posted 7 January 2016 (Doc. ID 254663); published 5 February 2016

The design, fabrication, and characterization of a label-free Mach–Zehnder interferometer (MZI) optical biosensor that incorporates a highly dispersive one-dimensional (1D) photonic crystal in one arm are presented. The sensitivity of this slow light MZI-based sensor scales with the length of the slow light photonic crystal region. The numerically simulated sensitivity of a MZI sensor with a 16 μm long slow light region is 115,000 rad/RIU-cm, which is sevenfold higher than traditional MZI biosensors with millimeter-length sensing regions. An experimental bulk refractive index detection sensitivity of 84,000 rad/RIU-cm is realized and nucleic acid detection is also demonstrated.

OCIS codes: (280.1415) Biological sensing and sensors; (160.5293) Photonic bandgap materials; (310.6628) Subwavelength structures, nanostructures; (260.3160) Interference.

http://dx.doi.org/10.1364/OL.41.000753

Label-free biosensors that transduce the presence of specific target molecules based on their capture by surface immobilized bioreceptors, as opposed to labeling of the target analytes with fluorescent or radiative tags [1], promote simple analyte preparation and real-time monitoring of specific binding interactions. Consequently, label-free biosensors are thought to hold the most promise for point-of-care diagnostics. Various photonic label-free biosensors have been developed to deliver portable, fast, accurate, and sensitive diagnostics, such as ring resonators [2–6], photonic crystal cavities [7–11], surface plasmon resonators [12,13], and Mach–Zehnder interferometers (MZIs) [14–18].

MZIs have been among the most sensitive biosensors as the relative phase shift between the two arms of a MZI is highly sensitive to refractive index perturbations. A typical on-chip MZI biosensor consists of two waveguide arms excited by a coherent single mode input source. The sensing arm has a window allowing interaction with biomolecules. The reference arm is usually protected by cladding material and inaccessible to the molecules. Molecular attachment results in an effective index change to the propagation mode in the sensing arm, causing a phase change that can be detected when the interference fringes change in the output optical spectra. MZI biosensors supporting increased light–matter interaction, such as MZIs with slot waveguides [17] and porous silicon MZIs [18], have been proposed and demonstrated for enhanced detection sensitivity, compared to traditional MZI biosensors. However, both conventional unbalanced MZIs [14,15] and the modified MZIs share the same challenge: a large footprint. Compared to micrometer-sized optical biosensors, such as photonic crystals (PhC) and microring resonators, the active sensing area of MZI sensors is usually on the order of millimeters. To solve this size challenge, we employ the slow light effect in a MZI via an added one-dimensional (1D) PhC to squeeze light and increase the relative phase shift per unit length in the sensing arm. The group index of the PhC near the band edge can be engineered to be very large, leading to a significant decrease in the group velocity of light. Additionally, the air holes of the photonic crystal increase the available surface area for biomolecule binding. Therefore, light–matter interaction in the slow light MZI is greatly enhanced due to both increased temporal interaction and a larger spatial overlap between the optical mode and target molecules. Recently, similar slow light MZIs have been proposed as a platform for optical modulators [19,20] and demonstrated for ultra-high speed optical signal modulation as a result of the enhanced phase-shift sensitivity [20]. In this Letter, we make use of the improved phase-shift efficiency of a silicon slow light MZI to realize a highly compact and sensitive device for optical label-free biosensing. We demonstrate in theory and experiment that the sensitivity of the slow light MZI biosensor scales with the sensing arm length. A fivefold detection sensitivity improvement, along with a 400 times reduction in footprint, is experimentally shown for the slow light MZI, compared to a traditional MZI sensor.

Figure 1(a) shows a schematic of the slow light MZI with the PhC incorporated in the sensing arm. Two different PhC designs were investigated, one with a circular unit cell and the other with a rectangular unit cell. The slow light performance of these two 1D PhC nanobeams was first investigated numerically to determine the most favorable geometry for sensing applications and integration in the MZI. Three-dimensional

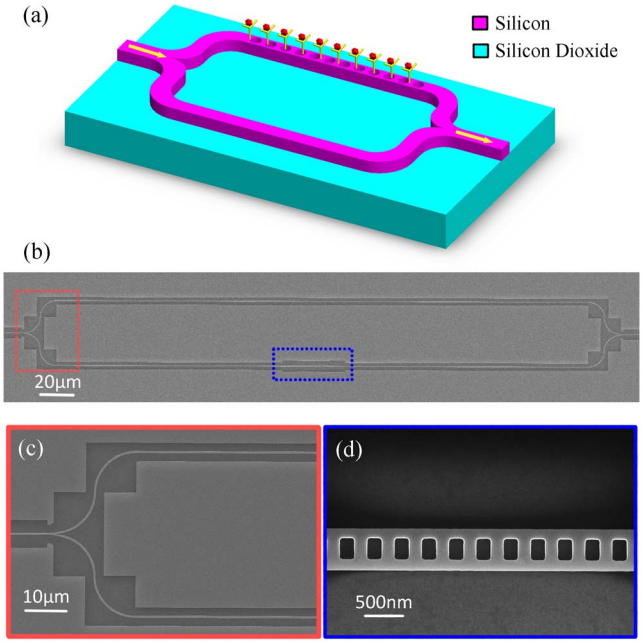

Fig. 1. (a) Schematic illustration of slow light MZI. The magenta structure indicates the silicon slow light MZI waveguide, and the cyan slab shows the silicon dioxide substrate. (b) SEM image of fabricated slow light MZI structure. The red box highlights the input splitter, and the blue box highlights the slow light PhC region. (c) SEM image of the splitter region where input light is divided 50/50 into the two arms of the MZI. (d) SEM image of the slow light PhC waveguide with rectangular holes.

finite-difference time-domain (FDTD) simulations (Lumerical, Inc.) were carried out to set the parameters of the PhCs to support a single guided mode near 1.55 μm. The appropriate period of the circular and rectangular air holes was found to be 360 nm. The radius of the circular air holes was set to 130 nm, and the rectangular air hole length and width were selected to be 300 nm and 200 nm, respectively. The width of the waveguide was 520 nm.

Figure 2(a) shows the simulated transmission spectrum of circular unit cell and rectangular unit cell PhC nanobeams with 45 periods. The simulated slow light mode profiles of both designs [Figs. 2(c) and 2(d)] indicate that the field is primarily squeezed in the dielectric region between air holes. The group index n_g is extracted from the transmission spectrum using Eq. (1) derived from phase-matching conditions [21]:

$$n_g = \frac{\lambda^2}{2\Delta\lambda L}, \tag{1}$$

where λ denotes the operation wavelength at the photonic band edge, $\Delta\lambda$ is the distance between two adjacent peaks at the band edge, and L represents the length of slow light region. Group index contours extracted from the data in Fig. 2(a) are plotted in Fig. 2(b). The rectangular hole unit cell design yields a slightly higher group index than the circular hole unit cell design. With the same operating wavelength and lattice constant, the rectangular lattice hole unit cell allows a slightly larger dielectric region between lattice holes, where the field can be localized as compared to the circular lattice hole unit cell.

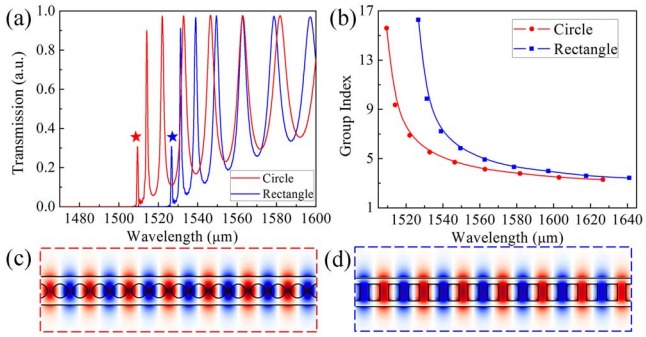

Fig. 2. (a) Simulated transmission spectra of slow light PhC waveguides with circular holes (red) and rectangular holes (blue). (b) Correspondingly derived group index contour of each PhC design. The propagation modes with the highest group index are marked by a star sign in (a), and their simulated mode profiles are shown in (c) and (d) for the circular hole and rectangular hole unit cell designs, respectively.

A slow light MZI incorporating a PhC nanobeam with rectangular air holes in the sensing arm was fabricated on a silicon-on-insulator (SOI) wafer with a top 220 nm silicon layer and a buried 3 μm oxide layer via electron beam lithography and reactive ion etching, similar to the process previously described in [5]. Figure 1(b) shows a scanning electron microscope (SEM) image of the fabricated slow light MZI, and Fig. 1(c) shows a magnified image of the splitter region. Light is divided into the two arms of the MZI in a 50/50 ratio and then recombined at the output using a splitter of the same design. Figure 1(d) shows a SEM image of the slow light PhC nanobeam in the sensing arm of the MZI. The length of the sensing arm is 16 μm.

Transmission measurements of the slow light MZI are carried out by coupling quasi-TE light from a tunable laser (SANTEC TSL-510) into the devices using lensed fiber (OZ Optics Ltd.). The output signal is detected by an optical power meter (Newport 1647). A comparison of the experimentally measured transmission spectrum and the simulated transmission of the same structure is shown in Fig. 3(a). There is good agreement near the peak of transmission; differences in the spectra at some wavelengths may arise from roughness of the fabricated devices and internal reflection at device boundaries, compared to the simulated one.

As an initial sensor benchmark, bulk sensitivity measurements are carried out to determine the spectral response of the slow light MZI to changes in the background refractive index when the structure is immersed in non-specific volumetric media. Note that due to the high index contrast and relatively short sensing length, the phase change of the reference arm is negligible, compared to that of the sensing arm, although they were given the same treatments in all studies. We further note that spectral measurements are carried out instead of the intensity-based, fixed wavelength measurements that are typically performed on conventional MZI structures. Spectral measurements not only provide more comprehensive information about the slow light transmission, but they are also necessary for slow light MZIs, since slow light structures must operate near the band edge and slow light MZIs require a relatively large index change to cause a sinusoidal variation of

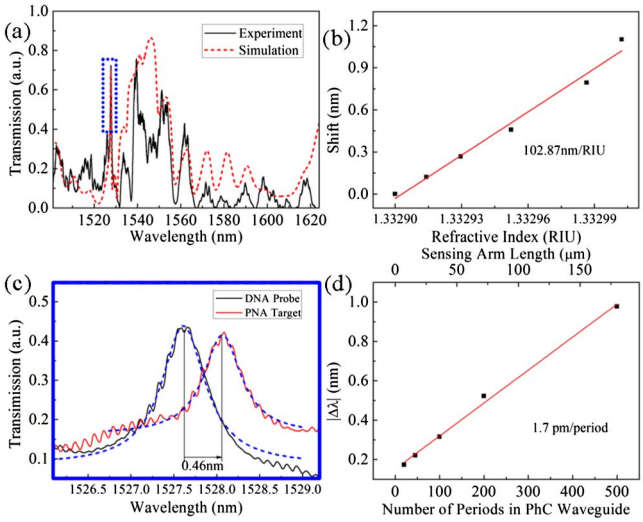

Fig. 3. (a) Simulated (red dashed) and experimentally measured (black line) transmission spectra of slow light MZI with rectangular holes. The peak used for sensing measurements is highlighted in the blue dotted rectangle. (b) Measured shift of transmission peak of slow light MZI upon exposure to different concentrations of salt water. A linear curve fit suggests a bulk detection sensitivity of 103 nm/RIU. (c) Transmission peak of slow light MZI in (a) (outlined by blue dotted box) after DNA probe attachment (solid black line) and PNA hybridization (solid red line). Lorentzian fits are shown as blue dashed lines. (d) Measured shift of transmission peak of slow light MZIs of different sizes after a 10-minute thermal oxidation at 500° C in air. The number of periods in the PhC waveguide in the sensing arms scales directly with the length of the MZI (shown on the top x axis).

transmission power (e.g., 2π phase change) at a fixed incident light wavelength. Various concentrations of salt water solutions (0.7–5.7 wt. %) are applied in this measurement. To avoid concentration fluctuation induced by solution evaporation, the fabricated device shown in Fig. 1(b) is integrated with a simple polydimethylsiloxane (PDMS) microfluidic cell, using a standard technique similar to that described in [22], which exposes the slow light MZI to the desired analyte. Salt water solutions are injected into the microfluidic channel at a constant rate of 5 μL/min. The refractive indices of the solutions range from 1.3329 to 1.3330, as measured by a birefringence refractometer (Leice Abbe II). Based on the data shown in Fig. 3(b), the bulk sensitivity is estimated to be 103 nm/RIU. This sensitivity is comparable to conventional silicon photonic MZI structures with sensing arms as long as 7 mm [15,18], SOI microring resonator-based biosensors [2] and photonic crystal cavity-based biosensors [9]. Hence, using the slow light effect, the device size can be 2 orders of magnitude smaller than conventional MZI sensors [15] while maintaining the same bulk sensing performance. We also numerically evaluated the bulk sensitivity of the slow light MZI using FDTD analysis by monitoring the simulated shift of the transmission spectrum as the background refractive index increases ($\Delta n_o = 0.001$). The simulated bulk sensitivity was found to be 140 nm/RIU, which is in reasonable agreement with the experiment, given slight fabrication variations between the simulated and fabricated structures.

Typically, the sensitivity of MZI sensors is reported in terms of a phase sensitivity that takes into account the length of the sensing arm. The phase sensitivity of an MZI is defined as [15]

$$S_{\text{phase}} = \frac{\Delta\varphi}{\Delta n \times L_S}, \tag{2}$$

where L_S is the length of the portion of the MZI sensing arm that is in contact with target biomolecules, and $\Delta\varphi$ is the phase shift caused by the refractive index change, Δn. Phase-matching conditions can be used to approximate the phase sensitivity based on the wavelength sensitivity:

$$S_{\text{phase}} = \frac{S_{\text{spectral}}}{\Delta\lambda \times L_S} \times 2\pi, \tag{3}$$

where S_{spectral} is the spectral sensitivity and $\Delta\lambda$ is the wavelength difference between two adjacent peaks in the slow light transmission spectrum from Fig. 2(a). Based on Eq. (3), we find that the simulated and experimental phase sensitivity is 115,000 and 84,000 rad/RIU-cm, respectively. The experimental phase sensitivity of the slow light MZI is fivefold higher, and the sensing arm length is 400 times smaller than conventional MZI biosensors [15].

Label-free detection of nucleic acid molecules is carried out next to experimentally demonstrate the surface sensing capability of the slow light MZI biosensor for the detection of specific target molecules using a simple drop cast method. The surface functionalization procedure used to prepare the MZI surface is similar to that described in [23,24]. First, the sample is thermally oxidized for 10 min at 500°C in air to passivate the surface with –OH terminations. The sample is next soaked in 1% 3-aminopropyltriethoxysilane (3-APTES) solution in toluene for 15 min. The sample is then the annealed at 150°C for 20 min to promote cross-linking among the 3-APTES molecules. Next, the heterobifunctional cross-linker, succinimidyl 3-(2-pyridyldithio)propionate (SPDP), prepared at a concentration of 2 mg/mL in ethanol, is drop casted onto the MZI surface and incubated for 30 min, followed by a soak in isopropanol for 5 min. The sample is then thoroughly rinsed with isopropanol and ethanol to remove unattached molecules. SPDP cross-links to the silanized MZI surface and to thiol-modified probe DNA. Before adding the probe DNA molecules to the sensor, a 10 μM solution of 16-mer probe DNA (5′-TAG CTA TGG TCC TCG T-3′, 3′ thiol C3, Eurofins MWG Operon) in deionized water is first reduced by using a TCEP resin. The DNA solution is then drop casted onto the sensor surface, incubated for 1 h, and then soaked in HEPES (4-(2-hydroxyethyl)-1-piperazineethanesulfonic acid) buffer for 20 min to remove non-specifically bound molecules. Finally, a complementary target PNA (5′-ACG AGG ACC ATA GCT A-3′) solution with a concentration of 10 μM is drop casted onto the MZI and incubated for 1 h. After hybridization, the device is soaked in HEPES buffer for 20 min to remove non-hybridized oligonucleotides.

Figure 3(c) shows, at the highlighted peak in Fig. 3(a), a transmission redshift of 0.46 nm resulting from the DNA-PNA hybridization. This result is comparable to sensing experiments performed on photonic crystal and micro-ring resonator structures under similar treatment conditions [5]. The limit of detection of those photonic crystals and micro-ring resonators was estimated to be in the nanomolar range.

For traditional MZI sensors, the spectral sensitivity scales with the size of the sensing arm. Longer sensing arms allow larger phase shifts to accumulate, which leads to a larger Fabry–Perot fringe shift at the output of the MZI. However, the increased detection sensitivity comes at the cost of an increased device footprint. The slow light MZI sensor presented in this Letter was designed with 45 periods of PhC holes in the sensing arm, which equates to a sensing arm that is only 16 μm long. To understand the trade-off between increased sensitivity and compact footprint, slow light MZIs with 20, 45, 100, 200, and 500 PhC periods are fabricated and characterized. The length of the reference waveguide arm of the MZIs is also changed accordingly. Each of the MZIs is oxidized at 500°C in air for 10 min, and their transmission spectra are subsequently measured. As shown in Fig. 3(d), the resulting peak transmission shift directly relates to the number of periods, or mirror segments, in the PhC. The detection sensitivity increases linearly such that the peak wavelength shift increases by approximately 1.7 pm/period for a given refractive index change as the length of slow light region increases. The refractive index change due to oxidation was estimated by ellipsometry. Approximately 1 nm ± 2 Å was grown, corresponding to a refractive index change of approximately 0.001. We note that the nonzero intercept of the linear fit in Fig. 3(d) is likely due to a slight asymmetry of the two MZI arms.

The dependence of the spectral sensitivity on the number of mirror segments can also be considered analytically. The number of mirror segments of the PhC is proportional to both the spectral sensitivity and length of the slow light region, while it is inversely proportional to the wavelength difference between two adjacent transmission peaks. By combining Eq. (3) and the phase-matching condition in the slow light region, the phase sensitivity of the slow light MZI can be written as

$$S_{\text{phase}} = \left(\frac{2mn_g}{\lambda} + \frac{1}{a}\right) \times \frac{2\pi k}{\lambda}, \tag{4}$$

where m is the number of segments; n_g is the localized group index at λ, the operation wavelength, which is approximately 1550 nm; a is the period or lattice constant of the slow light waveguide; and k is the slope extracted from the linear fit in Fig. 3(d) divided by the index change due to oxidation ($\Delta n_o \sim 0.001$). Equation (4) suggests that a slow light MZI with 10 mirror segments (<4 μm in length) is sufficient to achieve a detection sensitivity similar to that of a conventional 3 cm polymer MZI biosensor, as in [15].

In conclusion, a novel MZI integrated with a slow light PhC waveguide in the sensing arm has been designed, fabricated, and characterized in simulation and experiment. The 84,000 rad/RIU-cm experimental phase sensitivity of slow light MZIs with a 16 μm sensing arm is fivefold higher than traditional MZI biosensors, with a footprint that is two orders of magnitude smaller. Moreover, the detection sensitivity of the slow light MZI scales with sensing arm length, promising lower detection limits, compared to other resonator structures while maintaining a similar size.

Funding. National Science Foundation (NSF) (ECCS-0925642, ECCS-1407777).

Acknowledgment. This work was funded in part by the National Science Foundation. MZI fabrication was conducted at the Center for Nanophase Materials Sciences, which is a DOE Office of Science User Facility. Equipment usage and technical support at the Vanderbilt Institute for Nanoscale Science and Engineering (VINSE) and Vanderbilt Institute for Integrative Biosystems Research and Education (VIIBRE) is also acknowledged. The authors thank D. P. Briggs for assistance with sample fabrication, Y. Zhao for assistance with surface sensing, and P. Markov and G. A. Rodriguez for useful technical discussions.

REFERENCES

1. R. M. Lequin, Clin. Chem. **51**, 2415 (2005).
2. K. De Vos, I. Bartolozzi, E. Schacht, P. Bienstman, and R. Baets, Opt. Express **15**, 7610 (2007).
3. D.-X. Xu, M. Vachon, A. Densmore, R. Ma, A. Delâge, S. Janz, J. Lapointe, Y. Li, G. Lopinski, and D. Zhang, Opt. Lett. **35**, 2771 (2010).
4. A. J. Qavi, J. T. Kindt, M. A. Gleeson, and R. C. Bailey, Anal. Chem. **83**, 5949 (2011).
5. S. Hu, Y. Zhao, K. Qin, S. T. Retterer, I. I. Kravchenko, and S. M. Weiss, ACS Photon. **1**, 590 (2014).
6. G. A. Rodriguez, S. Hu, and S. M. Weiss, Opt. Express **23**, 7111 (2015).
7. M. R. Lee and P. M. Fauchet, Opt. Express **15**, 4530 (2007).
8. S. C. Buswell, V. A. Wright, J. M. Buriak, V. Van, and S. Evoy, Opt. Express **16**, 15949 (2008).
9. C. Kang, C. T. Phare, Y. A. Vlasov, S. Assefa, and S. M. Weiss, Opt. Express **18**, 27930 (2010).
10. M. G. Scullion, A. Di Falco, and T. F. Krauss, Biosens. Bioelectron. **27**, 101 (2011).
11. S. Chakravarty, Y. Zou, W.-C. Lai, and R. T. Chen, Biosens. Bioelectron. **38**, 170 (2012).
12. A. V. Kabashin, P. Evans, S. Pastkovsky, W. Hendren, G. A. Wurtz, R. Atkinson, R. Pollard, V. A. Podolskiy, and A. V. Zayats, Nat. Mater. **8**, 867 (2009).
13. N. C. Lindquist, A. Lesuffleur, H. Im, and S.-H. Oh, Lab Chip **9**, 382 (2009).
14. F. Prieto, B. Sepulveda, A. Calle, A. Llobera, C. Domínguez, A. Abad, A. Montoya, and L. M. Lechuga, Nanotechnology **14**, 907 (2003).
15. B. Sepulveda, J. S. Del Rio, M. Moreno, F. Blanco, K. Mayora, C. Domínguez, and L. M. Lechuga, J. Opt. A **8**, S561 (2006).
16. A. Crespi, Y. Gu, B. Ngamsom, H. J. Hoekstra, C. Dongre, M. Pollnau, R. Ramponi, H. H. van den Vlekkert, P. Watts, and G. Cerullo, Lab Chip **10**, 1167 (2010).
17. Q. Liu, X. Tu, K. W. Kim, J. S. Kee, Y. Shin, K. Han, Y.-J. Yoon, G.-Q. Lo, and M. K. Park, Sens. Actuators B **188**, 681 (2013).
18. K. Kim and T. E. Murphy, Opt. Express **21**, 19488 (2013).
19. A. Brimont, D. Thomson, P. Sanchis, J. Herrera, F. Gardes, J. Fedeli, G. Reed, and J. Martí, Opt. Express **19**, 20876 (2011).
20. H. C. Nguyen, Y. Sakai, M. Shinkawa, N. Ishikura, and T. Baba, Opt. Express **19**, 13000 (2011).
21. J. Y. Lee and P. M. Fauchet, Opt. Lett. **37**, 58 (2012).
22. X. Wei, J. W. Mares, Y. Gao, D. Li, and S. M. Weiss, Biomed. Opt. Express **3**, 1993 (2012).
23. K. R. Beavers, J. W. Mares, C. M. Swartz, Y. Zhao, S. M. Weiss, and C. L. Duvall, Bioconjugate Chem. **25**, 1192 (2014).
24. J. L. Lawrie, Y. Jiao, and S. M. Weiss, IEEE Trans. Nanotechnol. **9**, 596 (2010).